Characteristics of the extreme events observed in the Kerr-lens mode-locked Ti:sapphire laser

Alejandro A. Hnilo,[1,*] Marcelo G. Kovalsky,[1] Mónica B. Agüero,[1] and Jorge R. Tredicce[2]

[1]*Centro de Investigaciones en Láseres y Aplicaciones (CEILAP), CITEDEF-CONICET, J. B. de La Salle 4397, (1603) Villa Martelli, Argentina*

[2]*Pole Pluridisciplinaire de Materiaux et Energie (PPME), Université de la Nouvelle Caledonie, Nouméa, New Caledonia and Institute Non Linéaire de Nice (INLN), Université de Nice, UMR 7335, CNRS, Valbonne, France*

(Received 24 July 2014; revised manuscript received 17 November 2014; published 23 January 2015)

Kerr-lens mode-locked Ti:sapphire lasers are known to display three coexistent modes of operation: continuous wave, transform limited pulses (P1), and positive chirped pulses (P2). Extreme events (sometimes also called optical rogue waves), in the form of pulses of high energy appearing much often than in a Gaussian distribution, are observed in the chaotic regime of the P2 mode, but not of P1. The extreme events in P2 appear unpredictably, but their separation (measured in number of round trips) is a simple combination of the numbers 11 and 12 (which were named "magic numbers"). The existence of extreme events in P2 and not in P1, and also of the magic numbers, have been successfully reproduced by numerical simulations based on a five-variables iterative map, but the intuitive insight on the physical causes has been limited. In this paper, we present evidence that the extreme events in this laser appear if the amount of self-phase modulation on the pulses is above a certain threshold, and also that the P1 mode becomes unstable before crossing that threshold. This explains why the extreme events are observed in P2, and not in P1. Remarkably, even though the values of self-phase modulation on all the pulses (in the chaotic regime) are widely spread, the values inside the set of extreme events are relatively well defined. Finally, the magic numbers are found to be the residuals of the periodical orbits of the "cold" laser cavity when they are perturbed by the opposite effects of a dissipative term, due to the presence of transversal apertures, and an expansive term, due to the self-focusing.

DOI: 10.1103/PhysRevA.91.013836 PACS number(s): 42.65.Sf, 05.45.Tp, 05.45.Pq

I. INTRODUCTION

Waves of extremely high amplitude, appearing outside the Gaussian distribution, are important phenomena in deep ocean waters, and have received the name of "freak," or "rogue," waves [1]. In the last decade, scientific interest has increased on analogous rare or extreme events (EEs) of large amplitude observed in areas other than oceanography. In this sense, "optical rogue waves" were first observed in the light intensity fluctuations at the edge of the spectrum produced by ultrashort pulse pumped, microstructured optical fibers, in the threshold of supercontinuum generation [2,3]. Conditions for their formation were determined in experiments using optical fibers [4]. Optical EEs were observed in a Vertical Cavity Surface Emitting Laser (VCSEL) with an injected signal [5], in mode-locked fiber lasers [6–9], in all-solid-state lasers with a (slow) saturable absorber [10], and, what is of our interest here, in the Kerr-lens mode-locked (KLM) Ti:sapphire laser [11] (fast saturable absorber). A review on optical rogue waves has been recently published [12].

The quantitative definition of an EE usually is (a) amplitude higher than twice the "significant wave height" or "significant intensity" $I_{1/3}$ [7,8,13], which is the average calculated among the set of the one third highest events in the series [14]. An event is then considered "extreme" if its *abnormality index* $\mathrm{AI} \equiv I_{\mathrm{event}}/I_{1/3}$ is larger than 2. Alternatively, the definition is (b) amplitude higher than four times the standard deviation. These two definitions can be coincident or not, depending on the form of the distribution. The optical community has often employed the additional criterion of a long-tailed or L-shaped distribution. In previous contributions, we have also used the value of the kurtosis as an additional quantitative measure of a non-Gaussian feature. A value of the kurtosis larger than 3 means a distribution with a tail longer and higher than that of a Gaussian distribution. It provides an additional numerical criterion to classify a given dynamical regime as one with EE.

The KLM Ti:sapphire laser is the most widely used source of femtosecond (fs) light pulses nowadays. Its dynamics is intrinsically complex, because it is ruled by a balance of several spatial and temporal effects. In the temporal domain the group velocity dispersion (GVD) in all the optical components, and the intensity-dependent self-phase modulation (SPM), mostly in the laser rod, are balanced by the negative dispersion produced by an intracavity pair of prisms. In the spatial domain, the relevant effects are due to the cavity's geometrical configuration and the intensity-dependent self-focusing (SF). The amplification in the active medium is an additional source of nonlinearity through gain saturation. The pulse energy, the beam size, and the pulse duration are coupled by both the SPM and the SF effects. Three coexistent dynamical modes of operation are observed in the laser output if the total GVD is negative: continuous wave (cw), transform limited pulses (P1), and positive chirped pulses (P2). The laser spontaneously evolves from one mode to the other even in the absence of noise [15], and it is possible to induce a transition from one to the other by mechanical perturbations (say, by gently tapping a mirror mount). As the GVD of the laser cavity is adjusted close to zero from the negative side, the pulsed modes evolve towards chaos following a different route: P1 through quasiperiodicity, P2 through intermittency [16]. Be aware that what we call "mode" here means a *dynamical* characteristic of operation, not a spatial cavity mode (say, a Gauss-Laguerre mode). The

*ahnilo@citedef.gob.ar

laser is observed to oscillate in a single transversal spatial cavity mode.

Regarding the EEs observed in this laser, two phenomena appear especially intriguing:

(i) EEs are observed, and numerically predicted to occur, in the chaotic regime of P2, but not of P1.

(ii) Even though the appearance of a single EE seems to be unpredictable, preferred numbers (measured in cavity round trips, or intermediate non-EE pulses) are observed in the distance between successive EEs. We named them "magic numbers" [17].

Both phenomena are accurately reproduced by a numerical simulation based on a five-variables iterative map, yet, it provides limited insight on the physical causes. In this paper, we present evidence that the EEs in this laser appear if the average SPM crosses a certain threshold value. This result is in compliance with the report of different types of instabilities in fiber lasers [18]. We find that EEs are not observed in the P1 mode for, at the parameters' values beyond that threshold, this mode is unstable and the system rapidly evolves into the P2 mode. Finally, the magic numbers are due to the residuals of the periodic orbits of the "cold" laser cavity (i.e., the optical cavity without gain, losses, SF, or SPM) when it is perturbed by opposite dynamical effects.

The study of the EEs observed in KLM lasers, as a subject of dynamical systems, is interesting by itself. Besides, it will lead to a deeper understanding of the operation of these lasers and, eventually, to an improvement of their performance. KLM lasers may also provide a convenient test bench to study the general features of the phenomenon of EEs because laser dynamics evolves instantaneously (at the human time scale) and their control parameters are easy to adjust. One of the motivations to study oceanic rogue waves is the damage they inflict to ships or platforms. To the best of our knowledge, there are no reports on damage produced in optical systems by EEs in Ti:sapphire lasers. In this sense, it is fortunate that EEs exist only in the P2 mode, because the P1 mode is the preferred one in practice. It is also possible that damage produced by EEs in lasers have not been recognized as such.

In the next section, we review the necessary background. We describe the experimental setup where EEs are observed, and then we review the theoretical description with the five-variables iterative map. In Sec. III, we present evidence that the existence of EEs in this laser is consistent with the crossing of a threshold determined by the average value of the SPM, and we also explain why the EEs are observed in the P2 mode only. In Sec. IV, we consider the problem of the magic numbers.

II. BACKGROUND

A. The experiment: Setup and main results

The scheme of our Ti:sapphire laser is shown in Fig. 1. It is an X configuration, with a flat High Reflectivity (HR) rear mirror (M4) and a 12% output coupler (M1). The total cavity length is 1724 mm (round-trip frequency: 87 MHz). For a 5-W cw pump at 532 nm, the output power is 400 mW in the spectral region around 800 nm. Typical pulse durations in the uniform mode-locking regime are 35 fs (P1 mode) and 65 fs (P2 mode). We observe the mode-locking pulse train with a fast

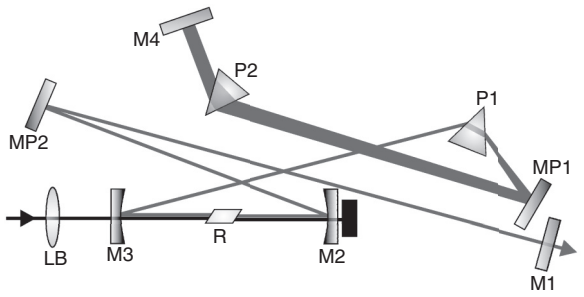

FIG. 1. Scheme of the laser. LB: pump focusing lens ($f = 10$ cm); $M_{2,3}$: curved mirrors ($R = 10$ cm); $MP_{1,2}$: plane HR mirrors; $P_{1,2}$: pair of prisms. Distances in mm: M_3–R = R–M_2 = 50, M_2–MP_2 = 140, MP_2–M_1 = 465, M_3–P_1 = 297, P_1–MP_1 = 198, MP_1–P_2 = 415, P_2–M_4 = 109. The prisms' positions are adjusted to get negative total GVD.

photodiode (0.2-mm diameter, 0.5-ns rise time) and record the signal in the memory of a high-speed sampling oscilloscope. Note that the photodiode is too slow to resolve the fs pulse shape—what we observe is the instrumental response to a "delta" input—and we then analyze the time series [16].

In the bistable region of the parameters, the laser wanders from one mode to the other in a time scale of several minutes. The modes can be distinguished by the pulse duration, the chirp, the spectrum, and even by the naked eye, as a change in the size of the laser spot. The pulses of the mode P1 are transform limited, and about half the length of the P2 ones [15]. EEs are easily observed in the chaotic regime of P2 (Fig. 2) [11]. Be aware that the experimental series is not an oscilloscope trace, but that each point represents the total energy of a single pulse, as it is obtained from the digitized experimental data by following the algorithm detailed in [16]. The theoretical series corresponds to the pulse energies calculated from the iterative map described in Sec. II B. On the right, a zoom of each series shows their detailed structure. The visible high-intensity peaks are caused by the periodicities of the cold optical cavity and are at the origin of the magic numbers, as explained in Sec. IV.

Typically, 100–200 pulses out of 10^4 are EEs. On the other hand, no EEs are observed in the chaotic regime of the P1 mode. This result supports the hypothesis of a nontrivial and deterministic nature of the observed EE. For, if the EEs in P2 were mere noise, or caused by self-Q-switching, there is no reason why they would not be observed in the coexisting P1 mode too. The theoretical approach based on the numerical running of a five-variables iterative map predicts the existence of EEs for P2 and not for P1, hence agreeing with the observations.

The hypothesis of a deterministic origin for these EEs is strengthened by the observation that, once inside the intermittent high-energy region, the EEs tend to appear at definite distances of each other [17]. Figure 3 shows the histograms of the distances between successive EEs, measured as the number of cavity round trips, for a representative time series. It is immediately seen that they are not uniformly distributed, but that they take only some preferred (magic) numbers: {11, 12, 23, 35, 46, 58, 94} in the experimentally obtained histogram, and {11, 12, 23, 24, 34, 35, 46, 58} in the

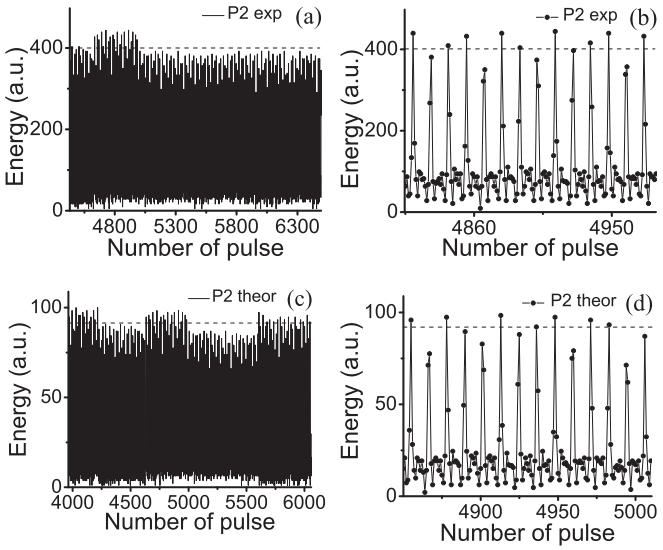

FIG. 2. Chaotic regime of the P2 mode. The horizontal dashed line indicates the threshold of EEs for the full time series according to the 2×AI criterion. (a) Experimental time series, zoom of ≈2000 pulses of 9978 with a total of 205 EEs, kurtosis = 4.91; (b) further zoom of the same; (c) theoretical time series obtained from the five-variables iterative map, zoom of ≈2000 iterations of 10^4 with a total of 226 EEs, kurtosis = 4.98; (d) further zoom of the same. Note the intermittent excursions to a regime of pulses of higher energy in both series. Be aware that each point in (b) and (d) is not the sample of a digital oscilloscope, but the energy of a single pulse in the mode-locking train. The periodicities behind the magic numbers (Sec. IV) are clearly visible. Average pulse duration: 80 fs.

theoretically obtained one. Note the remarkable coincidence between the experimental and the theoretical distributions. It is possible to predict the moment when an EE will *not* appear, despite the dynamics being chaotic. Note also that the magic numbers are simple combinations of 11 and 12. There are, however, missing combinations, as 22, 57, and 69 in both sets. Besides, there is an internal structure: If the distance between the n-EE and the $(n+1)$-EE is 11, there is a 93% probability that the distance to the $(n+2)$-EE is 12 (this probability is 77% in the theoretical series). In the same way, 23 follows 12 (with probability 82% both in the experimental and the theoretical series), 12 follows 23 (66% experimental and 40% theoretical), 23 follows 35 (61% experimental and 56% theoretical), and after 58 comes 35 in 100% of the cases (both experimental and theoretical). Second-step n to $n+2$ correlations also exist, but

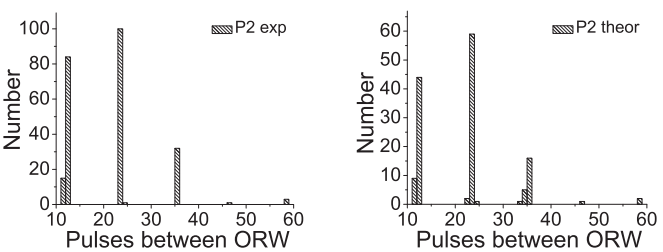

FIG. 3. Histograms of the number of EEs according to the distance (in cavity round trips) to the next EE in the chaotic regime of P2; left: experimental results; right: theoretical ones.

they are weaker. There is no correlation between the energy of an EE and its magic number [17].

The numerical coincidences between the experimental and the theoretical results indicate that these preferred numbers have a deep and robust cause, and that noise plays a minor role in the dynamics of EEs in this type of laser. It is to be noted that no fine-tuning of the many laser parameters has been performed in the numerical simulations. Tabulated and directly measured values have been used. Only the (negative) GVD has been adjusted, to fit the observed average pulse duration (80 fs, in this case).

B. The five-variables iterative map

The description of KLM lasers with iterative maps has been developed in several previous publications [15–17,19,20]. For completeness, it is briefly reviewed in the following lines. The reader familiar with this approach may skip this section.

The description with maps is alternative to that with a differential equation; no information is gained or lost. There are, however, some immediate advantages: The number of dimensions of the problem is reduced in (at least) one, the stability of the solutions is easily determined, and the numerical simulations run easier and faster. Period-doubling bifurcations are trivially described. However, writing the map equation can be as difficult as solving the differential equation, unless the physical system has some "internal clock" that determines the position of the adequate discrete times. In the case of KLM lasers, that clock is provided by the cavity round-trip time [19].

We suppose a Gaussian pulse, the electric field is given by $E(t) = E_0\exp(-ikr^2/2q)\exp(-ikt^2/2p)$ where r is the transverse distance to the optical axis; k is the wave number; and p, q are the usual beam parameters defined by the relationships [19,21]

$$1/q = n/R - 2i/k\sigma^2, \tag{1}$$

$$1/p = Q/k - 2i/k\tau^2, \tag{2}$$

where σ is the spot radius, R the beam curvature radius, τ the pulse duration, and Q the chirp (n is the index of refraction of the medium). This approximation is found valid for pulses longer than 20 fs [19]. As the pulse passes through an optical component (or propagates a distance), q changes according to

$$q_{\text{out}} = (\mathbf{A}\cdot q_{\text{in}} + \mathbf{B})/(\mathbf{C}\cdot q_{\text{in}} + \mathbf{D}), \tag{3}$$

where $\{\mathbf{A}\cdots\mathbf{D}\}$ are the elements of the usual 2×2 matrix of that component [21]. An analogous relationship holds for p [22]. The matrix describing the effect of the beam and pulse propagation through several optical components is obtained as the product of the matrices of each component. In standard cavities of KLM lasers, the general 4×4 round-trip matrix splits into two 2×2 diagonal blocks, which we call "spatial" [**ABCD**] and "time" [**KIJL**] matrices [19].

The $\{\mathbf{A}\cdots\mathbf{L}\}$ elements include factors that are functions of $\{\sigma,\tau\}$ and the pulse energy U. The factor due to SF is $\gamma = c_\gamma U/(\tau\sigma^4)$ and the one due to SPM is $\beta = c_\beta U/(\tau^3\sigma^2)$. The constants c_γ and c_β are proportional to the nonlinear index of refraction of the Ti:sapphire. Their precise expression is rather involved [23]. In our laser, they take the values $c_\gamma =$

1.38×10^{-11} cm^3 fs/nJ and $c_\beta = 2.18 \times 10^{-7}$ cm^2 fs/nJ. The values of these factors are different if the pulse crosses the Ti:sapphire rod in one direction or the other. We call $\{\gamma,\beta\}$ the factors that correspond to the case when the pulse propagates from M_3 to M_2 (see Fig. 1), and $\{\gamma',\beta'\}$ to the case when it propagates from M_2 to M_3.

The matrix elements are then written as a series expansion: $\mathbf{A} = A_0 + \gamma A_\gamma + \gamma' A'_\gamma + \cdots$ (the same for **B**, **C**, and **D**) being the coefficients of the expansion functions of the cavity's geometry. The time matrix is simpler: $\mathbf{K} = 1 + 2\beta'\delta$, $\mathbf{I} = 2\delta$, $\mathbf{J} = 2\beta'\beta\delta + \beta + \beta'$, $\mathbf{L} = 1 + 2\beta\delta$, where 2δ is the total GVD per round trip. Note that the $\{\gamma,\beta,\gamma',\beta'\}$ factors vanish in the limit of zero energy pulse. This defines the cold cavity limit. The equation for the pulse energy is obtained as an expansion of the condition of gain saturation [19]. Defining $S_n \equiv \sigma_n^{-2}$, $\rho_n \equiv R_n^{-1}$, and $T_n \equiv \tau_n^{-2}$, the expressions that link the pulse variable values at the $n+1$ round trip with the ones at the n round trip are [15,16]:

$$S_{n+1} = \frac{S_n}{(\mathbf{A} + \mathbf{B}\rho_n)^2 + (\mathbf{B}\lambda S_n)^2}, \tag{4a}$$

$$\rho_{n+1} = \frac{(\mathbf{A} + \mathbf{B}\rho_n)(\mathbf{C} + \mathbf{D}\rho_n) + \mathbf{BD}(\lambda S_n)^2}{(\mathbf{A} + \mathbf{B}\rho_n)^2 + (\boldsymbol{B}\lambda S_n)^2}, \tag{4b}$$

$$T_{n+1} = \frac{T_n}{(\mathbf{K} + \mathbf{I}Q_n)^2 + \left(\frac{\mathbf{I}T_n}{\pi}\right)^2} = T_n \frac{\mathbf{L} - \mathbf{I}Q_{n+1}}{\mathbf{K} + \mathbf{I}Q_n}, \tag{4c}$$

$$Q_{n+1} = \frac{(\mathbf{K} + \mathbf{I}Q_n)(\mathbf{J} + \mathbf{L}Q_n) + \mathbf{IL}\left(\frac{T_n}{\pi}\right)^2}{(\mathbf{K} + \mathbf{I}Q_n)^2 + \left(\frac{\mathbf{I}T_n}{\pi}\right)^2}, \tag{4d}$$

$$U_{n+1} = U_n \left\{1 - \frac{2(U^* S_n + U_n S^*)}{\mu D_s} + 4(\mu - 1)/\mu\right\}, \tag{4e}$$

where $\mu = 1.61$ is the product of the small signal gain Γ and the single passage feedback factor due to passive losses, and $D_s = 1.22$ mJ/cm^2 is the saturation energy multiplied by the cavity round trip. Here and in what follows, the asterisks indicate the values of the variables at a fixed point. The fixed points can be obtained analytically at first order in $\{\gamma,\beta,\gamma',\beta'\}$. If $t \to \infty$ then $\{\gamma,\beta,\gamma',\beta'\} \to 0$, which corresponds to the cw mode of operation. The condition $Q_n = Q_{n+1} = 0$ (i.e., zero chirp) leads to $\beta = \beta'$ and corresponds to the P1 mode (transform limited pulse) [15]. There is a fixed point with positive chirp, for which $\beta \gg \beta'$ (P2 mode) and one with negative chirp, for which $\beta \ll \beta'$ (P3 mode). The stability analysis of the fixed points explains why the P3 mode is not observed in practice [16].

For simplicity, we use three different forms of the map in the numerical simulations. In one of them the condition $\beta = \beta'$ is enforced, and hence it describes the evolution of the P1 mode only, as if the P2 mode did not exist. We call it the "P1 map." In the same way, the forced condition $\beta' = 0$ defines the "P2 map." A more involved numerical simulation, where β and β' evolve freely, is called the "bistable map" and is able to accurately describe the observed transitions from one mode to the other [20].

Each mode follows its own route to chaos. The calculated bifurcations diagrams in the energy variable are displayed in Fig. 4. The period-three stable window of P1 at ≈ -50 fs^2 was observed by Bolton and Acton [24]. In practice, the bistable

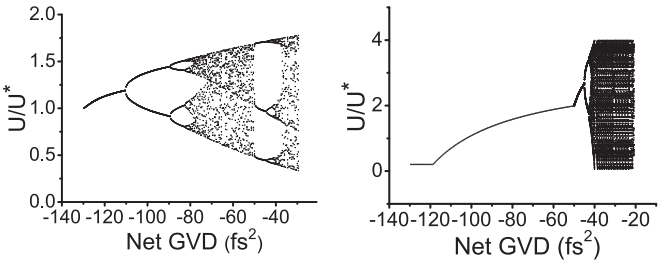

FIG. 4. Bifurcation diagrams for the pulse energy of the modes P1 (left) and P2 (right) as the GVD is varied, as obtained from their own five-variables maps. The energy is scaled to U^*; the fixed point energy value of P1 at GVD = –130 fs^2.

region spans between –60 and –40 fs^2. Near –38 fs^2 the P1 mode destabilizes into self-Q-switching, while the P2 mode does it near–20 fs^2. The observed self-Q-switching regime puts a limit to the validity of the description with this iterative map. The large excursions in energy of the P2 mode in its chaotic regime correspond to the existence of EEs (note the different vertical scales).

III. THE CAUSE OF THE OBSERVED EXTREME EVENTS

A. The SPM instability threshold

Early observations [11,17] and some results for fiber fs lasers [18] suggested that a high value of the SPM could be related with the formation of EEs in this laser. The value of the SPM acting on each pulse in a chaotic mode-locked train cannot be reliably measured in practice. Fortunately, we have at hand the five-variables iterative map which, as it was shown above, accurately reproduces the effects of interest here. The calculated values of β provide a measure of the amount of SPM on each pulse when crossing the laser rod. In Fig. 5, the calculated values of β and U (the total energy) for each pulse in a train of 10^5 are plotted, for each of the two modes, in the

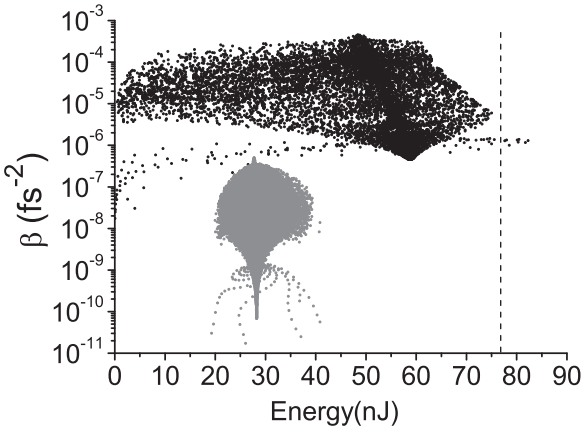

FIG. 5. Calculated values of β (a measure of the SPM) and the energy; each point represents one pulse of a chaotic time series of 10^5 after removal of a transient of 3×10^4. Note that almost all the pulses of the P2 mode (in black) have a larger value of β than even the largest ones of the P1 mode (in gray). The total number of EEs (the points to the right of the vertical dotted line) is 331, they seem to be fewer because of the scale of the figure. GVD = –42 fs^2.

region where both modes are chaotic (GVD = –42 fs^2). All the parameters correspond to the operation values of the real laser.

The P1(P2) map is used to calculate the points that correspond to the P1(P2) mode. The EEs are the dots at the right of the vertical dotted line; note that they belong to the P2 mode only. Even though the P2 pulses are spread over a large area in the diagram, the EEs all have practically the same value of β. We call this value $\beta_{EE} \approx 10^{-6}\,\mathrm{fs}^{-2}$. Curiously, β_{EE} is relatively low for the P2 mode. The pulses of the P1 mode, instead, accumulate in a small "cloud," below β_{EE}. The spiraling orbit corresponding to a quasiperiodical excursion, typical of the P1 mode, is noticeable.

Except for a few pulses of very low energy (on the left), the whole population of the P2 mode has a larger value of β than the highest of the P1 mode. It seems, then, probable that the P2 mode displays an EE because it is above an instability threshold related with the value of the SPM on the pulses. We speculate that the order of magnitude of this threshold, if measured with β, is given by β_{EE}. No pulse in the P1 mode is above β_{EE} in Fig. 5, but some of them are just at the border. A small increase in the pulse energy U should allow the P1 mode to cross the threshold too. We therefore increase the small signal gain Γ in the P1 map to increase the pulse energy, and plot histograms of the new energy pulse distributions. A 10% increase of Γ [Fig. 6(b)] changes the shape of the distribution [compare with Fig. 6(a)]: a central maximum appears and a high-energy tail starts to develop. For a 20% increase the tail is longer [Fig. 6(c)] and, for a 40% increase, EEs appear at last.

As a further check, the values of β,U for P1 are plotted in Fig. 7. In comparison with Fig. 5, the form of the P1 cloud has changed and most of the pulses are above $\beta_{EE} \approx 10^{-6}\,\mathrm{fs}^{-2}$ now, as expected. The β values of the set of EEs are much less

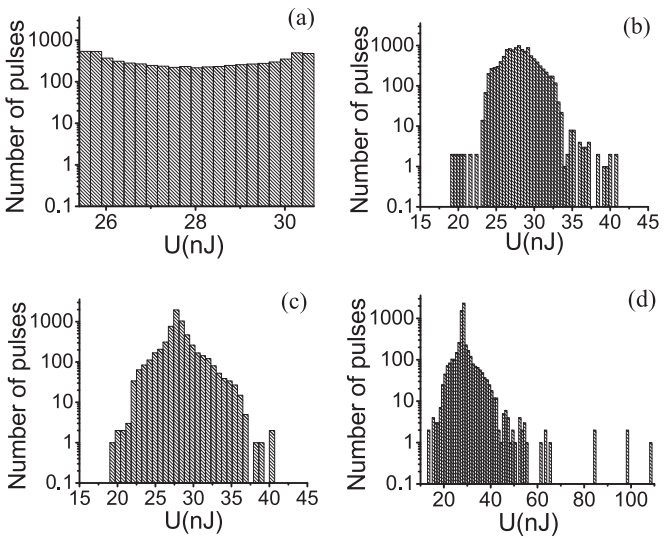

FIG. 6. Energy histograms (total 10^4 pulses) in the chaotic regime of the P1 mode for increasing small signal gain Γ, GVD = –42 fs^2 (a) at the normal operating value of the small signal gain, $\Gamma = \Gamma^*$; (b) $\Gamma/\Gamma^* = 1.1$; (c) $\Gamma/\Gamma^* = 1.2$, (d) $\Gamma/\Gamma^* = 1.4$; a total of 16 EEs are observed, kurtosis = 4.55. For (a–c), the value 2×AI is higher than 100 nJ and out of the figure, for (d) 2×AI = 63 nJ.

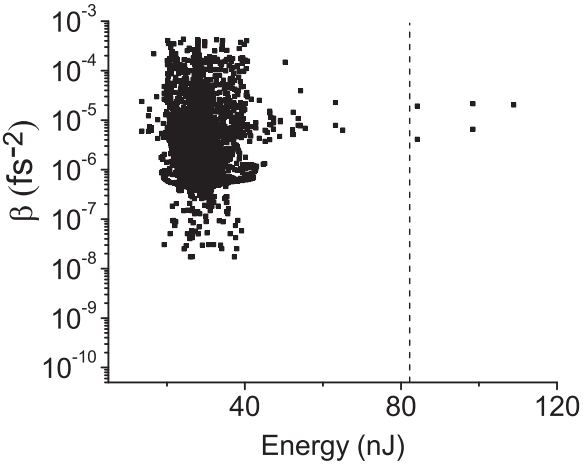

FIG. 7. β and the energy as in Fig. 5 but for the P1 mode only, and $\Gamma/\Gamma^* = 1.4$. Note the changes in shape and position of the cloud, and the appearance of EEs. The total number of EEs (the points to the right of the vertical dotted line) is 16; they seem to be fewer because of the scale of the figure.

spread than for the whole set of pulses, as in Fig. 5. Yet, in this case they are near the average β value instead of near the minimum.

B. Stability of the P1 mode in the regime with EEs

The natural conclusion at this point is that EEs should be observed also in the P1 mode if the small signal gain were increased. Nevertheless, this does not occur. We operate the laser under many different pump focusing and alignment conditions. In no case do we observe EEs in the P1 mode, and in all cases we observe them easily in the P2 mode. A hint to explain this result is that the volumes of the basins of attraction and the change of the eigenvalues, as the laser parameters are varied, indicate that the P1 mode is generally less stable than the P2. This numerical result is confirmed in the practice of this laser's operation.

Therefore, we run a numerical simulation with the bistable map and $\Gamma/\Gamma^* = 1.4$, and follow the pulse evolution. An example is shown in Fig. 8. The initial condition (U = 19 nJ, $\sigma = 39\,\mu$m, $\tau = 19$ fs, $Q = 0$) is very close to the fixed point of the P1 mode. The pulses in the P1 mode are the cloud on the left, and the ones in the P2 mode are the cloud on the right; note the different average values of the pulse variables in each cloud. After a few hundred iterations, corresponding to some μs of real time, and precisely at the point of a large excursion in the energy (the pulse energy reaches thrice the fixed point value), the system crosses from the P1 region to the P2 region, and remains there (where it does display EEs, note the vertical spread of the dots). After many runs like this, we see that in no case does the system remain in the P1 mode for a time long enough to be observed in practice.

As a further check, we plot in Fig. 9 the values of β and that of the largest (in modulus) eigenvalue, both for P1 and P2, as a function of the small signal gain. For P2, β crosses $\beta_{EE} \approx 10^{-6}\,\mathrm{fs}^{-2}$ before its largest eigenvalue crosses 1, while the opposite occurs for P1. We conclude that EEs are not observed in the P1 mode because this mode is unstable, against

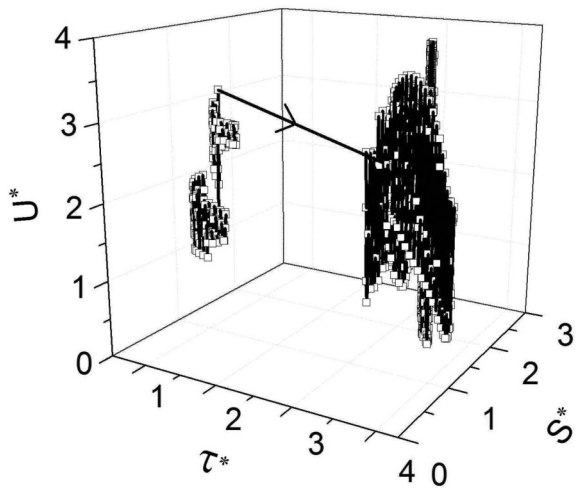

FIG. 8. Evolution of the pulse starting in the P1 mode (on the left) towards the P2 mode (on the right). All the parameters correspond to the operation point of the actual laser, except $\Gamma/\Gamma^* = 1.4$. Note that a high-energy excursion in P1 (an EE?) is followed by a transition to P2, where the system remains and displays EEs. The transition to P2 occurs after 218 round trips (≈2.5 μs in real time); total length of the run: 10^4 pulses. The variables are scaled to the fixed point of P1.

the coexisting P2 mode, if the gain is above the instability threshold.

The SPM-related instability that produces EEs in this laser is conceivably of a specific nature, still to be determined. We just mention a possible link to the modulational instability (MI) of the nonlinear Schrödinger equation. In physical terms, the MI arises when the (focusing) Kerr nonlinearity overwhelms the spread produced by the (negative) GVD scaled with the frequency of some harmonic perturbation. Then the perturbation grows exponentially, sidebands in the spectrum are generated by the nonlinearity, and, eventually, rogue waves are formed. The net value of GVD of our laser is negative, and the Kerr term is self-focusing, as required. A condition parallel to the MI can then be imagined, placing a threshold value to

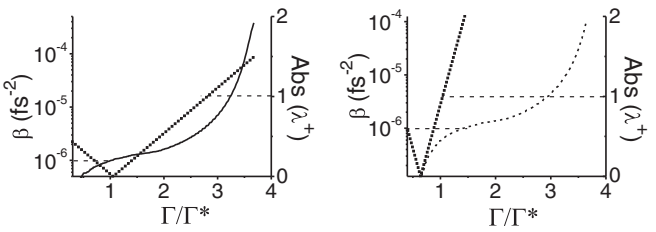

FIG. 9. Variation of β (curve, vertical axis on the left) and of the modulus of the largest eigenvalue (broken line, axis on the right) as a function of the scaled small signal gain Γ/Γ^*, for the modes P2 (left) and P1 (right); GVD = –42 fs^2. For P2, the SPM crosses $\beta_{EE} \approx 10^{-6}$ fs^{-2} at $\Gamma/\Gamma^* < 1$, while the largest eigenvalue crosses 1 (and the mode becomes unstable) at $\Gamma/\Gamma^* \approx 2.5$. Thus, at $\Gamma/\Gamma^* = 1$ the P2 is stable and displays EEs, as observed. Instead, for P1 the eigenvalue is >1 at $\Gamma/\Gamma^* \approx 1.1$ (and the mode becomes unstable) and SPM > β_{EE} at $\Gamma/\Gamma^* \approx 1.4$. Thus, EEs are not observed in P1 because this mode becomes unstable before reaching the instability threshold.

the Kerr nonlinearity (here, the SPM). An experimental result suggesting that the EEs in this laser follow a process similar to the MI is that spectral sidebands are observed in the P2 mode, and not in P1 [11].

IV. THE CAUSE OF THE QUASIPERIODICITIES

A. Changes if the threshold value of EE is lowered

As discussed before, the distance between successive EEs measured in round trips is observed to be a simple combination of the numbers 11 and 12. The threshold that defines an EE is rather arbitrary. If this threshold is lowered, "new" EEs appear intermediate of the old ones, always at a distance that is a combination of 11 and 12, depopulating the higher magic numbers. For example, an experimental time series generates the histogram of Fig. 3(a) if the threshold is established, following the 2×AI criterion, as 87 arbitrary units (a.u.). The total number of EEs is 237 and the magic numbers are {11,12,23,35,46,58,94}. If the threshold is lowered to 80 a.u., the number of EEs increases to 328 and the set is now {11,12,23,24,35}. If the threshold is further lowered to 75 a.u., the number of EEs increases to 397, the magic numbers 24 and 35 disappear, and the number 1 appears in the set (i.e, there are two successive EEs). The same phenomenon occurs in the theoretical time series, with a remarkable numerical coincidence with the observed ones. It is evident that a robust quasiperiodical phenomenon is underlying, with a typical period related with 11 and 12 round trips, regardless of the specific numerical value given to the threshold defining an EE.

B. Periodicities of the spatial part of the map

The evolution of the spatial part of the pulse (i.e., its beam size and curvature radius) in a cold cavity is known to be a periodical phenomenon [21]. It is therefore a natural candidate to explain the origin of the observed quasiperiodicities of the EE. In order to study this possibility, it is convenient to use a simpler form of the iterative map, which has been discussed in detail in Refs. [25,26]. We review here the essential points. The **ABCD** cold-cavity round-trip spatial matrix of Sec. II B can be transformed so that it has only two independent parameters: $A \equiv (A_0 + D_0)/2$ (with no units) and B_0 (units of length). Be aware of the differences between **A** (the element of the spatial matrix including SF and SPM), A_0 (the same but without SF and SPM) and A (just defined). Using B_0 to scale the beam parameter q in Eq. (1), such that $\psi_n \equiv B_0/q$, Eq. (3) becomes

$$\psi_{n+1} = A - (A + \psi_n)^{-1}. \tag{5}$$

The real part of the complex variable ψ_n is hence proportional to the inverse of the beam's radius of curvature, and the imaginary part to the inverse of the spot area (both in the n iteration). The fixed points of this map are $\pm i(1–A^2)^{1/2}$; one of them is physically meaningful and corresponds to the actual stable mode of the cavity. The other one is physically meaningless [21]. The expression for the map after n iterations starting from an arbitrary initial condition ψ_0 is [25]

$$\psi_n = \left(P_1^n + P_2^n \psi_0\right) / \left(P_2^n + P_3^n \psi_0\right), \tag{6}$$

where the P_j^n are polynomials in A, similar to Legendre polynomials. If $P_3^n = 0$ then $P_1^n = 0$ and $P_2^n \neq 0$ (see the

Appendix), and the solution becomes n periodic for any initial condition. It is then sufficient finding the zeros of P_3^n to know the periodicities of the cold cavity. The P_3^n polynomials and their roots until $n = 13$ can be found in the Appendix.

The two fixed points of the map Eq. (5) have indifferent stability. By taking into account that transversal apertures unavoidably exist (due to the finite diameter of the mirrors, of the pumped region, etc.), the physically meaningful fixed point becomes definitely stable, and the unphysical one, unstable [21]. The effect of an aperture of radius $R_{\rm ap}$ is taken into account in Eq. (5) by adding a term $-ia$, where $a = B_0\lambda/\pi R_{\rm ap}^2$. The effect of this term is dissipative: The map converges to the physically meaningful fixed point as $n \to \infty$, for all the initial conditions.

The effect of a self-focusing Kerr nonlinearity is taken into account with a term $-K_S \times S_n$, where K_S is approximated as a constant that includes the pulse intensity and the nonlinear index of refraction [26]. This means an important limitation in comparison with the five-variables map and the actual situation (see Fig. 2), where K_S varies. In spite of this limitation, this approximation allows a simple understanding of the origin of the magic numbers, as it is explained in what follows. Recalling that S_n (i.e., the inverse of the spot area at the n iteration) is proportional to the imaginary part of ψ_n, the map including the spatial effects of the apertures and the (approximate) SF is, from Eq. (5),

$$\psi_{n+1} = A - (A + \psi_n)^{-1} - ia - K_S \mathrm{Im}(\psi_n). \qquad (7)$$

The numerical study of Eq. (7) shows that, if $A > 0$, the map converges to the physically meaningful fixed point [26]. Its basin of attraction covers almost the whole complex plane if $a = 0$, and the whole plane if $a > 0$. If $A < 0$ instead, at least one of the Lyapunov exponents is positive and the iterations of the map diverge. Therefore, if $A < 0$ and $a, K_S > 0$, there are two tendencies in opposition: The effect of the aperture is to converge to the fixed point, while the effect of the nonlinear term is to diverge from it. Depending on the values of $\{a, K_S\}$ the map converges to the fixed point, diverges, or converges to periodic orbits of low periodicity. The latter can occur only if $a, K_S S_n \ll 1$, i.e., if the last two terms in Eq. (7) are small perturbations of the cold cavity.

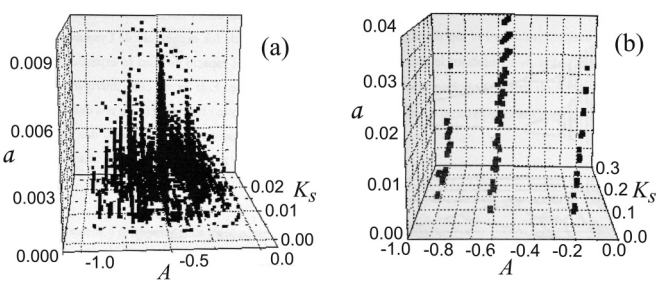

FIG. 10. (a) Values of $\{a, A, K_S\}$ that produce stable periodical orbits (period < 100) in the map [Eq. (7)]. Each dot represents an orbit, the fringed pattern is due to the accumulation of the orbits near the values of A that are zeros of P_3^n of low order. (b) The same as (a) but orbits of period 7 are plotted only; note that they are close to the zeros of P_3^7: $\{\pm 0.223, \pm 0.624, \pm 0.901\}$ (from Ref. [27]).

In Fig. 10(a), each dot indicates the set of values of $\{a, A, K_S\}$ producing a periodic orbit in Eq. (7). The set of dots accumulate in vertical lines or "fringes" close to the values of A that are zeros of polynomials P_3^n of low order. The effect is seen more clearly in Fig. 10(b), where only the perturbed orbits of period 7 are plotted. Note that all the orbits are near the zeros of P_3^7 (see the Appendix) and that they gently shift as $\{a, K_S\}$ increase. In other words, the orbits arising from the balance between the opposite tendencies of the Kerr effect and the aperture have a period equal to the n of the $P_3^n(A)$ of lowest order that has a zero near the value of A of the laser cavity.

In our opinion, this numerical result is quite intuitive. The periodic orbits of the cold cavity survive, modified, to the presence of the two opposite perturbations. The low-periodicity orbits dominate, after a sort of Darwinian selection, because their iterations are more distant in the complex plane than the ones with higher periodicity, and are hence more robust against the "blurring" of the trajectories caused by the perturbations.

C. The numbers of the real laser

In our laser, the Kerr effect is a small perturbation and there are no tight transversal apertures into the cavity. Therefore, the condition that the last two terms in Eq. (7) must be small is surely fulfilled. The numerical evaluation of the average value of K_S using the complete five-variables map supports this conclusion. The values of the elements of the round-trip matrix for the cold cavity are $A_0 = 4.1381$, $B_0 = 2.3048$ cm, $C_0 = 8.3276\,\mathrm{cm}^{-1}$, $D_0 = -4.3965$, so that $A = -0.1292$ (they can be calculated from the data in Fig. 1). Hence, the condition $A < 0$, $K_S > 0$ that defines opposite tendencies for the aperture and the Kerr effect is fulfilled too. Finally, the lowest P_3^n polynomial having a zero close to $A = -0.1292$ is P_3^{11} (the zero is -0.142; see the Appendix; the next closest zero of low order is -0.174, of P_3^9). This means that the cold cavity is close to the condition of periodicity 11. It is then reasonable to expect that the "hot" cavity displays orbits with a periodicity near 11, which is precisely what is observed both in the lab and in the numerical simulations with the complete (i.e., K_S not constant) five-variables map.

It remains to explain why there is nearly one pulse of higher energy than the average in each orbit. The iterations of the cold cavity (i.e., $a, K_S = 0$) lie on a circle in the complex plane of ψ_n, which is defined by the initial condition ψ_0. This circle passes between the fixed point and the origin of the complex plane [25]. The iterations are not equally spaced on this circle. There is "almost always" (it depends on the initial condition ψ_0) at least one iteration in the region between the fixed point and the origin, that is, a region of large spot area. A larger spot means a better overlap with the pumped region, and hence a larger value of U_n [see Eq. (4e)]. This means that, almost always, there is at least one pulse of higher energy per period. The perfect periodical process of the cold cavity is perturbed by the opposite effects of the aperture and the SF, but it survives in the form of the magic numbers. The perturbations also blur (and erase) the critical dependence on the initial condition.

To check this explanation, we modify the values of the geometrical parameters of the cavity and see if the magic numbers change accordingly. We choose $A = -0.225$, which

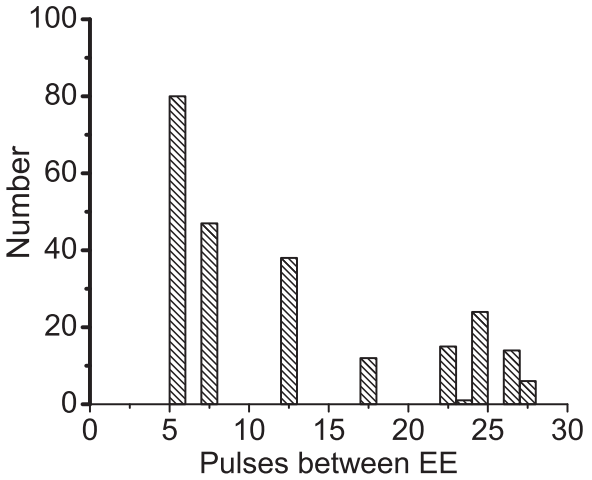

FIG. 11. Histogram of the number of EEs according to the distance (in cavity round trips) to the next EE, for the cavity modified such that A is a zero of P_3^7 and P_3^5; the other laser's parameters are the same as in Fig. 3. The magic numbers are now simple combinations of the numbers 5 and 7, as expected. The total number of pulses in this run is 15 000 and there are 239 EEs.

is a root of both P_3^7 and P_3^5. This leads to new values of the cold cavity parameters: $A_0 = 4.1860$, $B_0 = -2.3048\,\mathrm{cm}$, $C_0 = 8.5058\,\mathrm{cm}^{-1}$, $D_0 = -4.4444$. These values are inserted in the five-variables P2-map and new numerical simulations are run, all the other parameters' values being the same as before. Figure 11 displays the histograms for a run of 15 000 pulses, with a total of 239 EEs. As it is seen, the magic numbers are now {5, 7, 12, 17, 22, 23, 24, 26, 27, 121 (out of the figure)}. Leaving aside 23, with only one EE, these new magic numbers are simple combinations of 5 and 7, which are the periodicities of the orbits of the cold cavity for the value of A chosen. If the threshold for an EE is lowered, the larger magic numbers disappear and the EEs are separated by even simpler combinations of 5 and 7, in a way analogous to what happened in the original cavity. Analogous results are obtained for other values of A tested close to other zeros of the P_3^n of low order.

We conclude then that the observed quasiperiodicities of the EEs in this laser are the residuals of the stable geometrical orbits of the cold cavity, when perturbed by the opposite tendencies of a transversal aperture and SF.

V. SUMMARY

The chaotic regimes of the bistable KLM Ti:sapphire laser display a large variety of interesting dynamical behaviors, whose exploration is far from being completed here. We have focused on two intriguing features: (i) Why EEs appear in the chaotic regime of only one of the two pulsed modes of operation (the chirped-pulse mode or P2), and (ii) the cause of the discontinuous distribution of the separation between two successive EEs (the magic numbers).

Regarding (i), evidence is presented that the EEs appear if the average value of the SPM on the pulses is above a certain threshold, which we numerically estimate as $\beta_{\mathrm{EE}} \approx 10^{-6}\,\mathrm{fs}^{-2}$. This result is in general accordance with the instabilities reported in fs fiber lasers [18], and it may have a link with the MI. The crossing of that threshold occurs first for the P2 mode compared to the P1, for the average SPM on the pulses is larger for the former. Increasing the small signal gain in the P1 map makes the laser to cross that threshold and to display, *numerically*, EEs too. Yet, the EEs are not *observed* because the P1 mode is unstable at the increased value of the gain. In fact, the simulations with the bistable map show that, in spite of starting at the fixed point of P1, the laser evolves rapidly (in a scale of μs in real time) into the P2 mode, where it remains and does display EEs. In other words: no EE in the P1 mode is observed, because P1 becomes unstable (and the laser evolves into P2) before reaching the EE threshold. This result is fortunate for this laser's users, but pulses of very high energy are possible anyway during a transient (as in Fig. 8). It is therefore advisable in practice to block the laser cavity if the pump power or any other parameter is to be changed, even if the laser is running in the P1 mode.

A curious result is that the EE pulses take values of β that are much less spread than those of the whole set of pulses. This means that the EEs occur inside a relatively well defined region in phase space (say, a "β-constant" manifold). This result gives some hope to predicting, and eventually controlling, the formation of EEs. We foresee further research along this line.

Regarding (ii), the magic numbers are the residuals of the periodic orbits of the cold cavity, perturbed by the opposite tendencies of an expansive Kerr nonlinearity and dissipative losses. This result is easily explained with a simplified theoretical approach that reduces the KLM evolution, from the complete five-variables map, to an approximate map in the complex plane. The fact that the EEs in this laser are generally unpredictable, but that they can occur at only preferred times, is a further confirmation of their deterministic (i.e., not noise driven) nature. Note that it is not possible to predict when an EE will occur, but at least it is possible to predict when it will *not* occur. This can be considered as a step towards their complete forecast and control.

In this paper, we have studied the KLM Ti:sapphire laser as an object of dynamical interest. Nevertheless, the knowledge obtained from this study may prove helpful to improve the performance of this most used device and, hopefully, to shed some light on some general features of the formation of EEs.

ACKNOWLEDGMENTS

This work was supported by Grant No. FA9550-13-1-0120, "Nonlinear dynamics of self-pulsing all-solid-state lasers" of the AFOSR (USA); Contract No. PIP2011-077 "Desarrollo de láseres sólidos bombeados por diodos y de algunas de sus aplicaciones" of the CONICET (Argentina); and the project OPTIROC of the ANR (France).

APPENDIX

The $\mathrm{P}_{\mathrm{j}}^n$ polynomials are linked by the formation relationships: $P_1^n = (A^2 - 1)P_3^n$ and $P_3^n = A\,P_3^n - P_3^{n-1}\,P_3^{n-1}$, so that all of them can be calculated knowing the P_3^n. The general form of the P_3^n is detailed in [25]. The first P_3^n polynomials are $P_3^1 = -1$, $P_3^2 = 2A$, $P_3^3 = 4A^2 - 1$, $P_3^4 = 8A^3 - 4A$. The following ones can be calculated from the recursive equation: $P_3^{n+1} = 2A\,P_3^n - P_3^{n-1}$.

A P_3^n polynomial has n–1 zeros. The values of the zeros of the P_3^n until order $n = 13$ are as follows: $n = 1$: none; $n = 2$: 0; $n = 3$: $\pm\frac{1}{2}$; $n = 4$: 0, $\pm 1/\sqrt{2}$; $n = 5$: ± 0.223, ± 0.901; $n = 6$: 0, $\pm\frac{1}{2}$, $\pm\sqrt{3}/2$; $n = 7$: ± 0.223, ± 0.624, ± 0.901; $n = 8$: 0, ± 0.329, $\pm\sqrt{2}/2$, ± 0.924; $n = 9$: ± 0.174, $\pm\frac{1}{2}$, ± 0.766, ± 0.940; $n = 10$: 0, ± 0.309, ± 0.588, ± 0.809, ± 0.951; $n = 11$: ± 0.142, ± 0.415, ± 0.654, ± 0.840, ± 0.960; $n = 12$: 0, ± 0.259, $\pm\frac{1}{2}$, $\pm\sqrt{2}/2$, $\pm\sqrt{3}/2$, ± 0.966; $n = 13$: ± 0.120, ± 0.350, ± 0.566, ± 0.748, ± 0.883, ± 0.971.

[1] C. Kharif, E. Pelinovsky, and A. Slunyaev, *Rogue Waves in the Ocean* (Springer-Verlag, Berlin-Heidelberg, 2009).

[2] D. Solli, C. Ropers, P. Koonath, and B. Jalali, Optical extreme events, Nature **450**, 1054 (2007).

[3] C. Finot, K. Hammami, J. Fatome, J. Dudley, and G. Millot, Selection of extreme events generated in Raman fiber amplifiers through spectral offset filtering, IEEE J. Quant. Electron. **46**, 205 (2010).

[4] A. Montina, U. Bortolozzo, S. Residori, and F. T. Arecchi, Non-Gaussian statistics and extreme waves in a nonlinear optical cavity, Phys. Rev. Lett. **103**, 173901 (2009).

[5] C. Bonatto, M. Feyereisen, S. Barland, M. Giudici, C. Masoller, José R. Rios Leite, and J. R. Tredicce, Deterministic optical extreme events, Phys. Rev. Lett. **107**, 053901 (2011).

[6] J. M. Soto-Crespo, P. Grelu, and N. Akhmediev, Dissipative rogue waves: Extreme pulses generated by passively mode-locked lasers, Phys. Rev. E **84**, 016604 (2011).

[7] A. Zaviyalov, O. Egorov, R. Iliew, and F. Lederer, Rogue waves in mode-locked fiber lasers, Phys. Rev. A **85**, 013828 (2012).

[8] C. Lecaplain, P. Grelu, J. M. Soto-Crespo, and N. Akhmediev, Dissipative rogue waves generated by chaotic pulse bunching in a mode-locked laser, Phys. Rev. Lett. **108**, 233901 (2012).

[9] A. Runge, C. Aguergaray, N. Broderick, and M. Erkintalo, Raman rogue waves in a partially mode-locked fiber laser, Opt. Lett. **39**, 319 (2014).

[10] C. Bonazzola, A. Hnilo, M. Kovalsky, and J. Tredicce, Optical rogue waves in the all-solid-state laser with a saturable absorber: Importance of the spatial effects, J. Opt. **15**, 064004 (2013).

[11] M. Kovalsky, A. Hnilo, and J. Tredicce, Extreme events in the Ti:sapphire laser, Opt. Lett. **36**, 4449 (2011).

[12] J. Dudley, F. Dias, M. Erkintalo, and G. Genty, Instabilities, breathers and rogue waves in optics, Nat. Photonics **8**, 755 (2014).

[13] M. Erkintalo, G. Genty, and J. Dudley, On the statistical interpretation of optical rogue waves, Eur. Phys. J.: Spec. Top. **185**, 135 (2010).

[14] H. Svedrup and W. Munk, Wind, sea and swell. Theory of relations for forecasting, US Navy Hydrographic Office, Technical Report Number 1, Hydrographic Office Publication Number 601, March 1947.

[15] M. Kovalsky, A. Hnilo, A. Libertun, and M. Marconi, Bistability in Kerr lens mode locked Ti:sapphire lasers, Opt. Commun. **192**, 333 (2001).

[16] M. G. Kovalsky and A. A. Hnilo, Different routes to chaos in the Ti:sapphire laser, Phys. Rev. A **70**, 043813 (2004).

[17] A. A. Hnilo, M. G. Kovalsky, and J. R. Tredicce, Extreme value events in self-pulsing lasers, in *Fifth Rio De La Plata Workshop on Laser Dynamics and Nonlinear Photonics, Colonia del Sacramento, 2011* (IEEE, Piscataway, NJ, 2011), pp. 1–3.

[18] F. Wise, A. Chong, and W. Renninger, High-energy fs fiber lasers based on pulse propagation at normal dispersion, Laser Photonics Rev. **2**, 58 (2008).

[19] A. Hnilo, Self mode locking Ti:sapphire laser description with an iterative map, J. Opt. Soc. Am. B **12**, 718 (1995).

[20] M. Kovalsky and A. Hnilo, Bistable behavior of a KLM Ti:sapphire laser, Int. J. Bifurcation Chaos Appl. Sci. Eng. **18**, 1719 (2008).

[21] A. Siegman, *Lasers* (University Science Books, Mill Valley, CA, 1986), Chaps. 20, 21.

[22] A. Kostenbauder, Ray pulse matrices: A rational treatment for dispersive optical systems, IEEE J. Quantum Electron. **26**, 1148 (1990).

[23] M. Marioni and A. Hnilo, Self starting of self mode locking Ti:sapphire lasers. Description with a Poincaré map, Opt. Commun. **147**, 89 (1998).

[24] S. R. Bolton and M. R. Acton, Quasiperiodic route to chaos in the KLM Ti:sapphire laser, Phys. Rev. A **62**, 063803 (2000).

[25] L. Sánchez and A. Hnilo, Optical cavities as iterative maps in the complex plane, Opt. Commun. **166**, 229 (1999).

[26] L. Sánchez and A. Hnilo, Description of Kerr lens mode locked lasers with Poincaré maps in the complex plane, Opt. Commun. **199**, 189 (2001).

[27] L. Sánchez, Dinámica de mode-locking por efecto Kerr, Ph.D. Thesis, Universidad de Buenos Aires, 2003.